

Patterns and magnitude of deep sea carbonate dissolution during Eocene Thermal Maximum 2 and H2, Walvis Ridge, southeastern Atlantic Ocean

Lucy Stap,¹ Appy Sluijs,² Ellen Thomas,^{3,4} and Lucas Lourens¹

Received 23 June 2008; revised 17 December 2008; accepted 29 December 2008; published 18 March 2009.

[1] Eocene Thermal Maximum 2 (ETM2 or H1; ~53.7 Ma) represents a short-lived warming episode, associated with the injection of a large mass of ¹³C-depleted carbon into the ocean-atmosphere system. The mass of injected carbon, the extent of deep sea dissolution, and the amount of warming during ETM2 appear to be approximately half of those documented for the Paleocene-Eocene thermal maximum (PETM, ~55.5 Ma), but the pattern of lysocline migration during ETM2 has not yet been documented sufficiently to decipher potential differences in carbon sources and sequestration mechanisms. We present high-resolution carbonate dissolution and bulk stable isotope records across ETM2 and the successive H2 event (~53.6 Ma) on a common age model for four sites along the Walvis Ridge depth transect (1500 to 3600 m paleowater depth) to assess lysocline evolution. The onset of ETM2 is characterized by multiple, depth-dependent transitions of carbonate dissolution (up to ~96% of the total flux), associated with rapid depletions in bulk carbonate carbon (up to ~1–1.5‰) and oxygen (up to ~0.7–1.5‰) isotope values. H2 shows a ~0.7‰ negative carbon isotope excursion, with a coeval decrease in $\delta^{18}\text{O}$ of ~0.5‰ and ~80% of carbonate dissolution. During ETM2, the lysocline recovered within ~30 ka. We attribute this rapid recovery to terrestrial CaCO₃ neutralization through enhanced chemical weathering of carbonates in soils and rocks. According to theory, carbonate dissolution was lower after recovery than prior to ETM2, indicating carbonate ion oversaturation and a deeper position of the lysocline. Spectral analysis indicates that the changes in carbonate dissolution and $\delta^{13}\text{C}$ values were precession paced, implying that weathering feedbacks and short-term perturbations in the carbon cycle were important in determining early Eocene background and hyperthermal ocean [CO₃²⁻] conditions.

Citation: Stap, L., A. Sluijs, E. Thomas, and L. Lourens (2009), Patterns and magnitude of deep sea carbonate dissolution during Eocene Thermal Maximum 2 and H2, Walvis Ridge, southeastern Atlantic Ocean, *Paleoceanography*, 24, PA1211, doi:10.1029/2008PA001655.

1. Introduction

[2] Superimposed on the late Paleocene through early Eocene warming was a prominent, short-lived warming phase referred to as the Paleocene-Eocene Thermal Maximum (PETM; ~55.5 Ma) [Kennett and Stott, 1991; Zachos et al., 1993]. This event was marked by a transient, pronounced negative excursion in stable carbon isotope ($\delta^{13}\text{C}$) in marine and terrestrial sedimentary components and severe deep sea calcium carbonate dissolution [e.g., Kennett and Stott, 1991; Thomas and Shackleton, 1996; Zachos et al., 2005; Schouten et al., 2007], indicative of the (rapid) release of large amounts of ¹³C-depleted carbon into the ocean-atmosphere system. Both the source of the carbon and mode of carbon injection are under vigorous debate

[Dickens et al., 1995, 1997; Kurtz et al., 2003; Svensen et al., 2004; Higgins and Schrag, 2006; Pagani et al., 2006; Sluijs et al., 2007a, 2007b; Moore and Kurtz, 2008]. Regardless of its source, the mass of carbon added was almost certainly > 2000 Gigatons [Dickens et al., 1997; Panchuk et al., 2008].

[3] The PETM may represent the extreme example in a series of similar events called hyperthermals [Thomas and Zachos, 2000; Lourens et al., 2005]. Stable carbon isotope records spanning the late Paleocene and early Eocene show numerous short-lived $\delta^{13}\text{C}$ depletions or transient excursions, termed A to L, and have been linked to maxima in the Earth's orbital eccentricity cycle [Cramer et al., 2003]. Recently it has been shown that the H1 excursion corresponds to a prominent warming event, and this event has been named Eocene Thermal Maximum 2 (ETM2; ~53.7 Ma) [Lourens et al., 2005]. The PETM and ETM2, as well as other short-lived transient events, may have been triggered by a similar orbital-related forcing mechanism [Lourens et al., 2005; Westerhold et al., 2007] and would therefore require a source that may have repeated carbon injections.

[4] During the PETM, significant environmental change slightly preceded the onset of the CIE, suggesting that the

¹Faculty of Geosciences, Utrecht University, Utrecht, Netherlands.

²Palaeoecology, Laboratory of Palaeobotany and Palynology, Institute of Environmental Biology, Utrecht University, Utrecht, Netherlands.

³Centre for the Study of Global Change, Department of Geology and Geophysics, Yale University, New Haven, Connecticut, USA.

⁴Also at Department of Earth and Environmental Sciences, Wesleyan University, Middletown, Connecticut, USA.

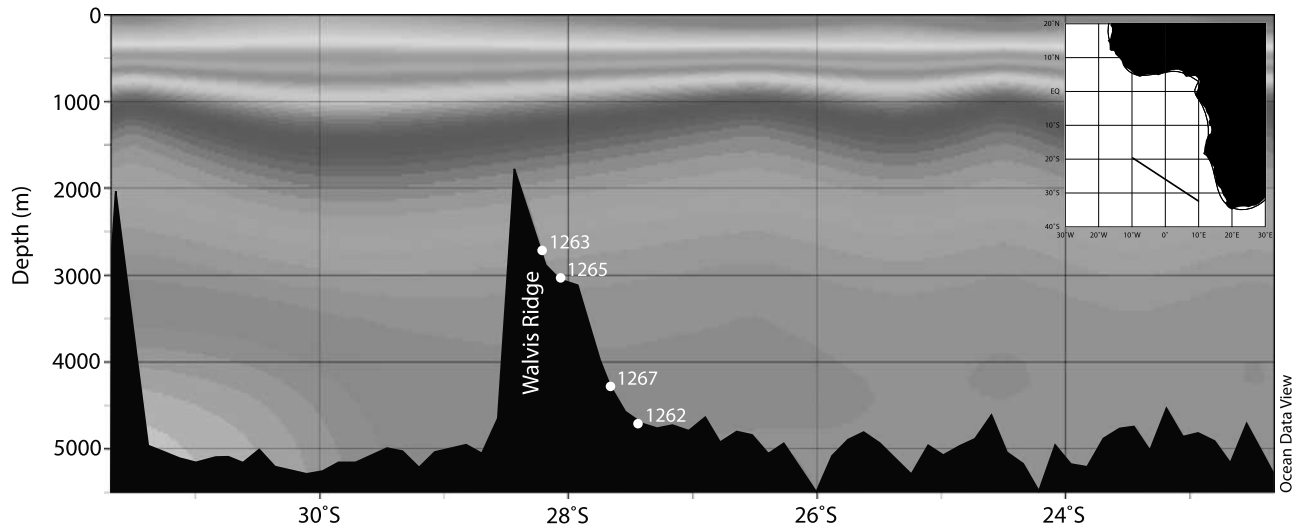


Figure 1. Transect through southeastern Atlantic Ocean showing the approximate locations of Sites 1263, 1265, 1267, and 1262. Shaded contours are modern water temperature (from R. Schlitzer, Ocean Data View, 2008, <http://odv.awi.de>).

CIE was in part a feedback reaction to already rapidly changing conditions [Shuijs *et al.*, 2007b]. Such a scenario is consistent with the release of methane hydrates [Dickens *et al.*, 1995], but similar detailed evidence is not yet available for ETM2, partially because no records with sufficient temporal resolution have been published. As yet, documentation of the presumed hyperthermals is insufficient to unravel whether they share a similar origin.

[5] Records of the PETM and ETM2 have been recovered during Leg 208 on Walvis Ridge (SE Atlantic Ocean, Figure 1). In the sedimentary record, these events are marked by distinct red clay-rich layers (in case of ETM2 referred to as the Elmo horizon) [Lourens *et al.*, 2005; Zachos *et al.*, 2005]. During the PETM, the lysocline and calcite compensation depth (CCD) shoaled by at least 2 km in this region [Zachos *et al.*, 2005]. The recovery was gradual, with the onset of increased carbonate preservation at the shallowest Site 1263 after ~10 to 15 ka of the CIE onset, only after ~60 ka at the deepest Site 1262. By ~110 ka, carbonate content had fully recovered at all sites, with carbonate concentrations higher than prior to the event. The magnitude of the CIE, degree of warming and decrease in carbonate content during ETM2 at Walvis Ridge were estimated to represent approximately half of those during the PETM [Lourens *et al.*, 2005]. Because of the lack of a common age model for each site, it has remained unclear, however, to what extent the pattern of dissolution and the CIE during ETM2 was depth-dependent as shown for the PETM [Zachos *et al.*, 2005; McCarren *et al.*, 2008]. Moreover, although Lourens *et al.* [2005] identified H₂ carbon isotope and dissolution records were not generated.

[6] Here we aim to fully assess the patterns, degree and timing of dissolution and the size and depth dependency of the CIE in bulk sediment during ETM2 and H₂ at Walvis Ridge. Therefore we generated high-resolution records of carbonate content, > 63 μm sediment fraction wt %, and bulk carbonate stable carbon and oxygen isotopes for four sites drilled during ODP Leg 208.

2. Materials and Methods

[7] ODP Leg 208 recovered sediment deposited during ETM2 at 5 sites along a 2 km depth transect on the northeastern flank of the Walvis Ridge [Lourens *et al.*, 2005] (Figure 1). Samples were used from ODP Sites 1263 (28°31.98'S, 02°46.77'E, 2717 water depth), 1265 (28°50.10'S, 02°38.35'E, 3060 water depth), 1267 (28°05.88'S, 01°42.66'E, 4355 water depth), and 1262 (27°11.15'S, 01°34.62'E, 4755 water depth) (Figure 2), with paleowater depths ranging from ~1500 m to 3600 m [Zachos *et al.*, 2004]. The sections were sampled continuously at 0.5–1.0 cm resolution and analyzed for carbonate content, coarse fraction wt % and bulk carbonate $\delta^{13}\text{C}$ and $\delta^{18}\text{O}$.

[8] For coarse fraction analysis, freeze-dried bulk sediment samples were weighed before they were gently rinsed over 150, 63 and 38 μm sieves. Subsequently they were oven-dried and the weight of all fractions determined. A decrease in the coarse fraction wt % may indicate a drop in preservation, because planktic foraminifera break apart into smaller fragments before complete dissolution [e.g., Schlanger and Douglas, 1974]. In pelagic sediments, however, where the major carbonate constituents are usually nanofossils, the coarse fraction wt % can be an imperfect dissolution proxy [Hancock and Dickens, 2006].

[9] The carbonate content of the freeze-dried bulk sediment samples was based on the amount of total carbon combusted with the Fison NA 1500 CNS analyzer. It was assumed that the total carbon was carbonate only, because no significant amount of organic carbon had been detected [Lourens *et al.*, 2005]. Calibration to international standard BCR-71 and in-house standard F-TURB, revealed an analytical precision better than 0.5% and 0.1% for C.

[10] Total magnetic susceptibility (MS) measurements of freeze-dried bulk samples were carried out with a Kappabridge KLY-2 magnetic susceptibility meter at Utrecht University and expressed in S.I. units per gram

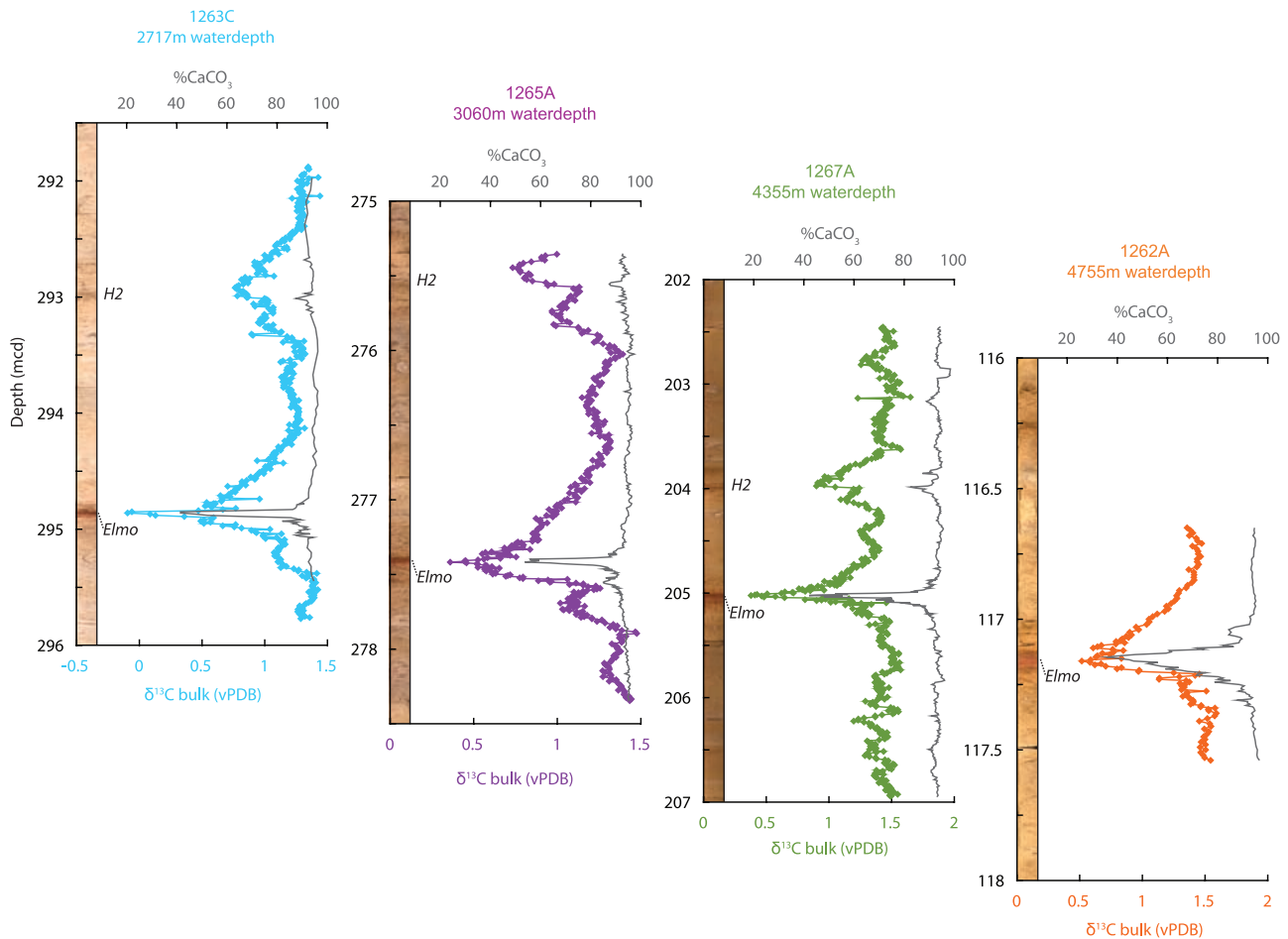


Figure 2. Bulk carbon isotope and carbonate content records for 1263C, 1265A, 1267A, and 1262A plotted versus depth (mcd).

sediment. MS is a sensitive indicator of variations in the concentration of terrigenous material relative to pelagic carbonate [Clemens and Prell, 1991; Verosub and Roberts, 1995], also at Walvis Ridge [Zachos et al., 2004] and can therefore be used to estimate CaCO_3 wt % [Lourens et al., 2005]. MS shows a less noisy pattern than the measured CaCO_3 wt %, probably caused by the larger and more uniform sample used for the MS analyses, and is therefore chosen to develop the age model. From a second-order polynomial fit between the paired analyses of CaCO_3 wt % and the MS/g we obtain the following estimated CaCO_3 wt % scale: $\text{CaCO}_3 \text{ wt \%} = -0.0084217468 * (\text{MS/g})^2 - 0.7341572721 * (\text{MS/g}) + 98.0980804665$, where $R^2 = 0.92$ and $n = 1068$. A comparison of the estimated and measured CaCO_3 wt % shows an error of 1%.

[11] Bulk stable isotope ratios were measured at Utrecht University with an ISOCARB common acid bath carbonate preparation device linked to a VG SIRA24 mass spectrometer. Calibration to the international standard NBS-19 and in-house standards IAEA-CO1 and NAXOS shows that analytical precision was better than 0.05‰ and 0.10‰ for $\delta^{13}\text{C}$ and $\delta^{18}\text{O}$ respectively. Stable isotope data presented include data generated in this study as well as previously

published data generated with the same equipment and procedures [Lourens et al., 2005].

[12] Spectral analysis was applied to the bulk carbon isotope time series of Sites 1263, 1265 and 1267 using the CLEAN algorithm [Roberts et al., 1987]. A Monte Carlo based method [Heslop and Dekkers, 2002] was used to determine the different levels of significance. The spectra were determined by (1) 10% (i.e., control parameter = 0.1) red noise addition, (2) clean gain factor of 0.1, (3) 500 CLEAN iterations, (4) dt value of 0.5 ka, and (5) a total number of simulation iterations of 1000.

3. Results

3.1. Age Model

[13] A relative age scale for each site was developed assuming a constant flux of terrigenous input and calcium carbonate production. This implies that the estimated sedimentation rates depend only on changes in CaCO_3 content due to preservation/dissolution processes. The maximum CaCO_3 content determined within the study interval was 96% at the shallowest sites. On this basis, we assumed the bulk sediment consists of 96% CaCO_3 and 4% terrigenous

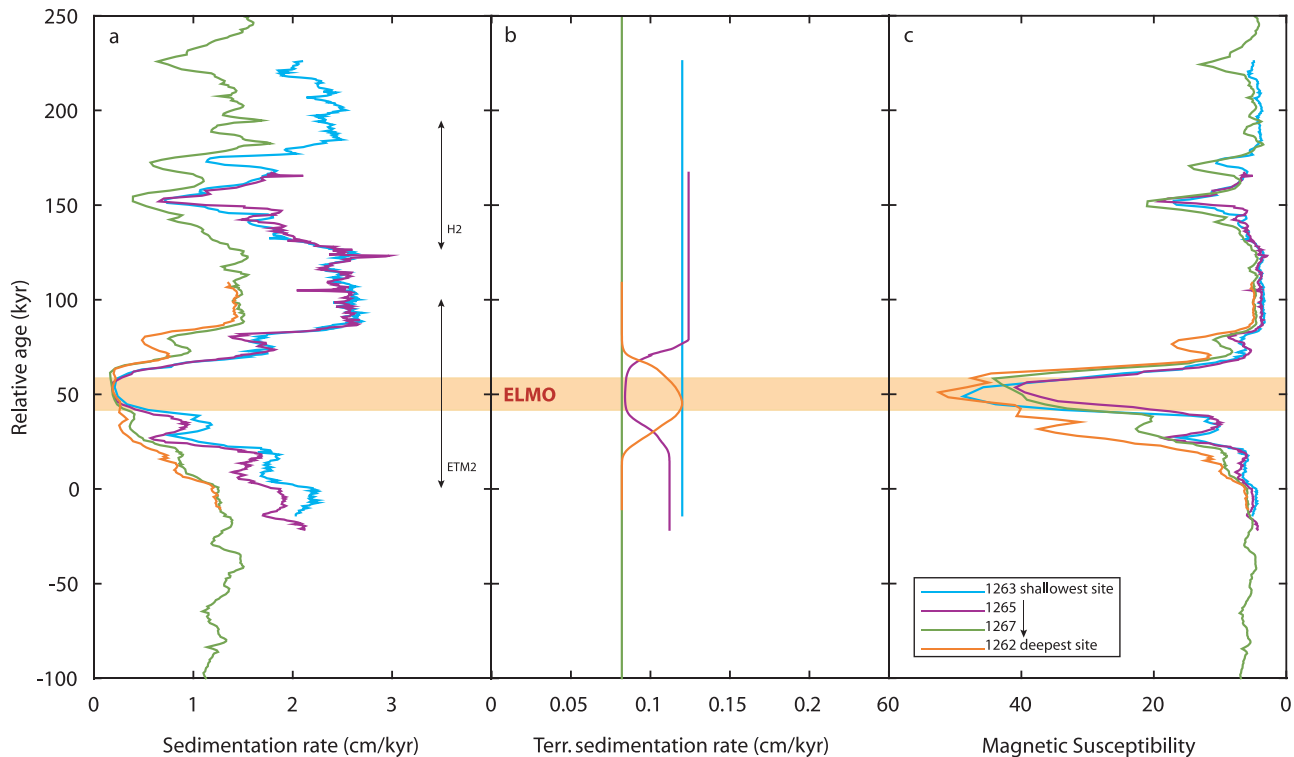


Figure 3. (a) Total sedimentation rates, (b) terrigenous sedimentation rates, and (c) magnetic susceptibility (MS) plotted versus relative age for Sites 1263, 1265, 1267, and 1262 during ETM2 (all sites) and H2 (Sites 1263, 1265, and 1267). The onset of ETM2 is set at a relative age of 0 ka. The smoothed changes in terrigenous sedimentation rates of Sites 1265 and 1262 are obtained by Gaussian fitting techniques.

material when all (100%) the produced CaCO_3 is preserved. The average sedimentation rate (and absolute value of the terrigenous flux) is finally constrained by the ~ 100 ka time interval (one short-term eccentricity cycle) between ETM2 and H2 [Cramer *et al.*, 2003; Lourens *et al.*, 2005; Westerhold *et al.*, 2007].

[14] We choose the shallowest Site 1263 as the backbone of our age scale, because it has the highest sedimentation rate as well as the most amplified CIE during ETM2 [Lourens *et al.*, 2005]. At this site we set the reference or zero point at 295.47 m composite depth (mcd), the approximate base of ETM2 [Lourens *et al.*, 2005]. Given a mean estimated CaCO_3 content of the studied interval of 93% and the ~ 100 ka duration of the time interval between the Elmo horizon (at 294.86 mcd) and H2 (at 293.01 mcd), we estimated a constant terrigenous flux of 0.12 cm per ka and an average total sedimentation rate of 1.76 cm per ka. Lowest sedimentation rates are within the Elmo horizon (0.27 cm per ka) and highest (2.6–2.7 cm per ka) between the Elmo horizon and H2 (Figure 3a).

[15] The same procedure was applied to the other sites. As reference points, we chose 277.935 mcd at Site 1265, 205.335 mcd at Site 1267 and 117.410 mcd at Site 1262. The absolute flux of terrigenous material as estimated for Site 1263 could not be applied to all sites, because this led to inconsistencies between the age scales of the resulting bulk isotope and CaCO_3 time series. Terrigenous fluxes

probably varied across Walvis Ridge, possibly reflecting changes in the terrigenous sources. During the early Paleogene, shallow locations received comparable fluxes of eolian and hemipelagic material, whereas deeper locations received mostly hemipelagic material [Nicolo and Dickens, 2006]. We therefore adopted slightly different values for the terrigenous flux at each site. This approach, however, did not fully resolve the offsets between the various time series, with largest discrepancies occurring within the Elmo horizon of Sites 1262 and 1265. Subsequently, we optimized the correspondence between the time series by gradually changing the terrigenous flux (partly using Gaussian fitting techniques) through the Elmo horizon of these sites until the best fit was achieved with Sites 1263 and 1267 (Figure 3). According to our age model, estimates of mean CaCO_3 content and sedimentation rates of the studied interval for Sites 1262, 1267, and 1265 are 85, 92 and 92%, and 0.8, 1.1 and 1.6 cm per ka, respectively. The systematic decrease in sedimentation rate with depth is consistent with more dissolution at the deeper sites. The average sample resolution is ~ 1 ka for Sites 1262 and 1267 and ~ 0.5 ka for Sites 1263 and 1265.

[16] The marked but minor adjustments in the terrigenous flux across the Elmo horizon of Sites 1265 (decrease) and 1262 (increase) may reflect coring disturbance, rather than true changes in terrigenous flux. In particular, the stiff clay horizon could have been relatively compressed with respect

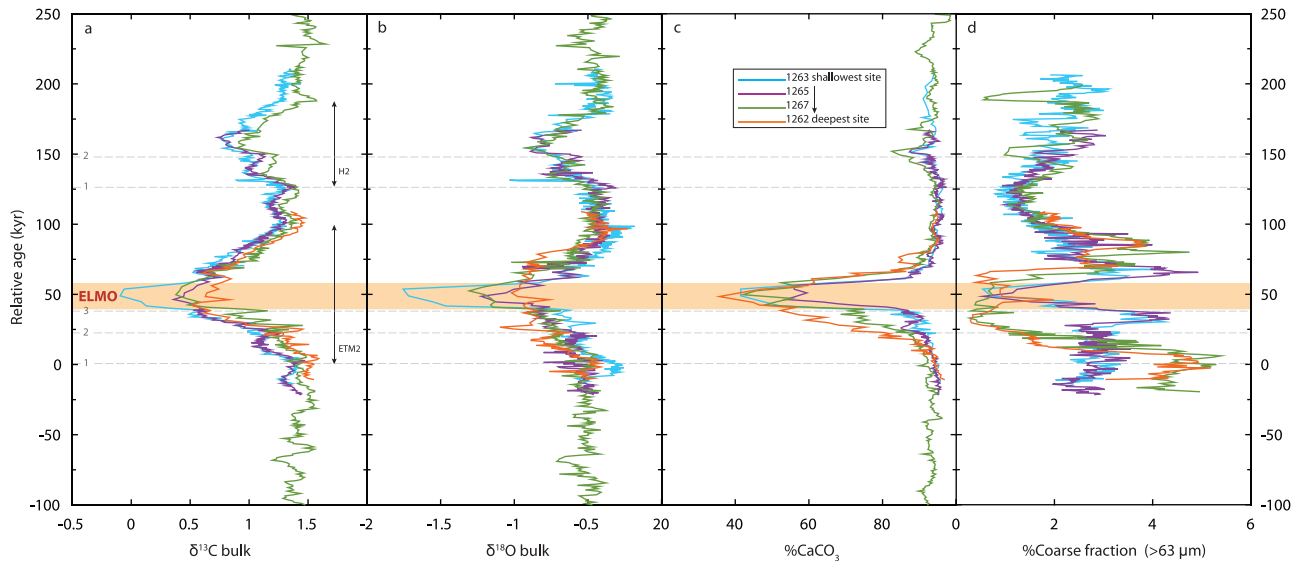


Figure 4. Bulk sediment (a) $\delta^{13}\text{C}$ and (b) $\delta^{18}\text{O}$, (c) carbonate content, and (d) the coarse fraction content plotted versus relative age for Sites 1263, 1265, 1267, and 1262. Gray lines indicate several $\delta^{13}\text{C}$ transitions during the onset of the events.

to the surrounding carbonate ooze during coring at Site 1265, but slightly more expanded at Site 1262. Although average terrigenous fluxes are probably well-constrained, short-term fluctuations are difficult to resolve. It can be argued that the terrigenous flux during deposition of the Elmo clay layer was higher than average, because of enhanced continental weathering rates as inferred for the PETM [Ravizza *et al.*, 2001; Shuijs *et al.*, 2008]. We tested this hypothesis by doubling the terrigenous flux during the Elmo horizon at all sites (not shown). The outcome of this test revealed no marked changes in the age model, because the terrigenous flux makes up only a very small part of the sediments studied, and the time interval between ETM2 and H2 is well constrained. Similarly, carbonate production may have varied, but there is also no direct evidence that this has played a significant role.

3.2. Bulk Stable Isotope Time Series

[17] The $\delta^{13}\text{C}$ values dropped rapidly by $\sim 0.4\text{‰}$ at all sites from the onset of ETM2, as defined by Lourens *et al.* [2005], at a relative age of 0 ka (Figure 4). At ~ 15 ka relative age, $\delta^{13}\text{C}$ increased again at all sites by 0.1–0.2‰, just before the major and second negative $\delta^{13}\text{C}$ transition of $\sim 0.8\text{‰}$ at ~ 23 ka. The total CIE of Sites 1262, 1267 and 1265, including both transitions, is about 1.0‰, with a coeval decrease in $\delta^{18}\text{O}$ of $\sim 0.7\text{‰}$ (Figures 2 and 4). Site 1263 is the only site at which the $\delta^{13}\text{C}$ and $\delta^{18}\text{O}$ values dropped by another $\sim 0.5\text{‰}$, at ~ 40 ka, concomitant with the onset of the Elmo horizon, resulting in a total $\delta^{13}\text{C}$ and $\delta^{18}\text{O}$ excursion of $\sim 1.5\text{‰}$. The recovery to baseline $\delta^{13}\text{C}$ values remained $\sim 0.2\text{‰}$ below pre-ETM2 values and took about 55 ka. The total duration of ETM2, as currently defined, approximates 100 ka.

[18] ETM2 was followed by another episode of decreasing $\delta^{13}\text{C}$, $\delta^{18}\text{O}$ and carbonate content at ~ 128 ka (Figure 4; cycle 0 in the work by Lourens *et al.* [2005]). This transient

excursion was observed and named H2 at other locations [Cramer *et al.*, 2003; Nicolo *et al.*, 2007]. The bulk isotope records at Sites 1263, 1265 and 1267 reflect a total depletion of $\delta^{13}\text{C}$ of $\sim 0.6\text{‰}$ and a coeval decrease in $\delta^{18}\text{O}$ of $\sim 0.5\text{‰}$ (Figure 4). Two transitions mark the CIE of H2: from the onset of H2, $\delta^{13}\text{C}$ values dropped by $\sim 0.4\text{‰}$, and then increased at all sites by 0.2‰ just before the second decrease by $\sim 0.4\text{‰}$ at ~ 150 ka. The full recovery to baseline $\delta^{13}\text{C}$ values took about 27 ka, arriving at a total duration of H2 of approximately 60 ka.

[19] The mean bulk carbon isotope values over the whole studied interval of Sites 1265, 1267 and 1262 are respectively $\sim 0.03\text{‰}$, $\sim 0.13\text{‰}$ and $\sim 0.17\text{‰}$ higher than at Site 1263 (Figures 4 and 5). Mean $\delta^{18}\text{O}$ values during ETM2 were lower by $\sim 0.2\text{‰}$ from the shallowest Site 1263 to the deepest Site 1262, but there is no $\delta^{18}\text{O}$ gradient between the sites during H2 in contrast to ETM2 (Figure 5).

3.3. Carbonate Dissolution

[20] From the onset of ETM2, carbonate contents at all sites decreased along with the $\delta^{13}\text{C}$ transitions, following a depth-dependent pattern with least dissolution at the shallowest Site 1263 (Figure 4). During the first transition, starting at 0 ka, the carbonate content declined only slightly (< 5 wt %). The second transition, at ~ 18 ka, is most pronounced, especially at the deeper Sites 1262 and 1267. At Site 1267, values dropped from ~ 92 (pre-ETM2) to ~ 73 wt %, then remained relatively stable. At the deepest Site 1262, values decrease almost continuously from $\sim 95\%$ at the onset of ETM2 to a minimum value of 36 wt % within the Elmo horizon (Figure 4). This second transition is less distinct at the shallower Sites 1263 and 1265 (from 94 to ~ 85 wt %), and is followed by a temporary recovery rather than a plateau. The third transition marks the base of the Elmo horizon at ~ 35 ka, where carbonate wt % decreased by more than 40 wt % at the shallower Sites 1263 and 1265,

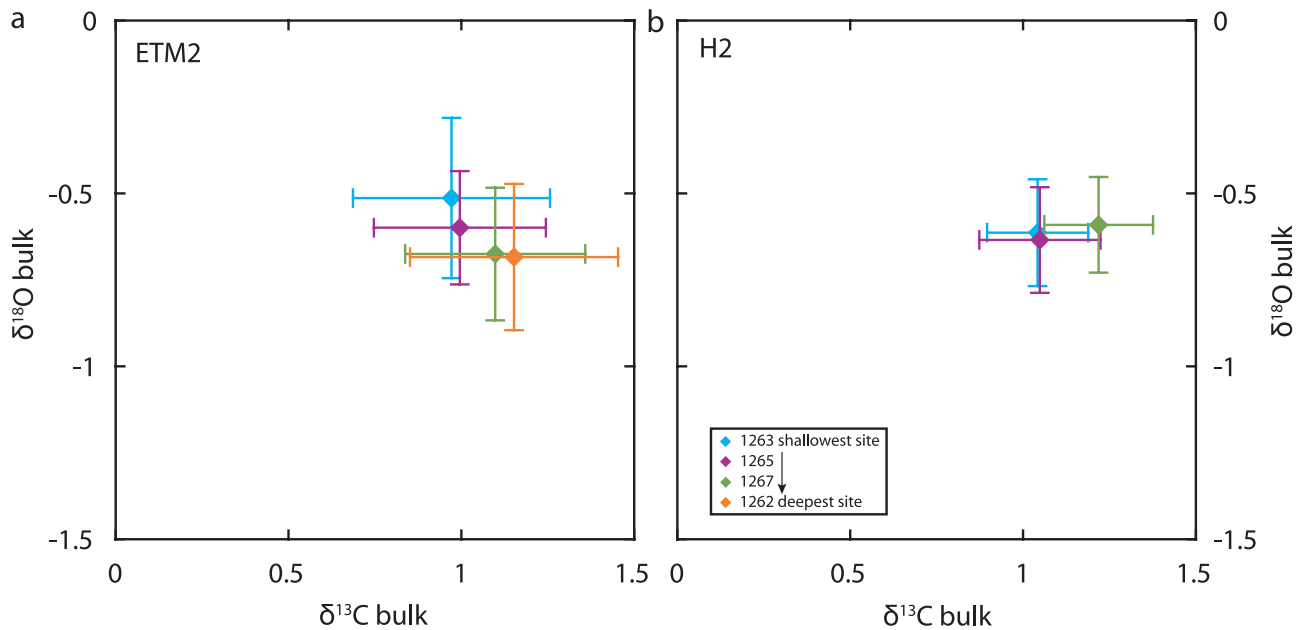


Figure 5. XY plots with the average $\delta^{13}\text{C}$ and $\delta^{18}\text{O}$ with their standard deviations. (a) ETM2 (0–100 ka) for Sites 1263, 1265, 1267, and 1262. (b) H2 (126–188 ka) for Sites 1263, 1265, and 1267.

and another ~ 20 wt % at the deeper sites 1262 and 1267. The lowest values of ~ 36 wt % are found in the Elmo horizon of Site 1262, followed by Site 1267 (~ 42 wt %), and the shallowest Site 1263 (~ 41 wt %). A marked exception in this depth-dependent dissolution pattern is the carbonate wt % record of the intermediate Site 1265, which shows less dissolution within the Elmo horizon than all other sites. Above the Elmo horizon, the carbonate content for all sites recovered to pre-ETM2 values within 30 ka, independent of depth. The decrease in carbonate content during H2 was on average less than 10 wt %, with a maximum decrease from ~ 95 to 83 wt % at Site 1267 (Figure 4). The recovery of the carbonate content to pre-H2 conditions occurred within 10 ka.

[21] To fully understand the pattern of CaCO_3 dissolution during ETM2 the closed sum effect between the CaCO_3 and terrigenous fluxes that biases observed changes in CaCO_3 wt % should be acknowledged [Broecker, 1995]. Our assumption that bulk sediment consists of 96 wt % CaCO_3 in absence of carbonate dissolution, implies that up to 96% of the total CaCO_3 flux is dissolved when the CaCO_3 content reaches 50 wt % (Figure 6). We used this relationship to estimate the part of the CaCO_3 flux dissolved over the studied interval. Although small changes in primary productivity or terrigenous flux will change the absolute estimate of carbonate dissolution (with up to a few percent), they will not significantly alter the pattern. Our reconstruction shows that changes in dissolution occurred synchronously between the sites with almost complete CaCO_3 dissolution within the Elmo horizon (95.1–97.6%). Throughout the studied interval, dissolution of up to 50% is a common feature of the background variation (Figure 6), but only within the Elmo and H2 horizons dissolution of more than 80% took place at all sites.

[22] The CaCO_3 dissolution decreased along with the three $\delta^{13}\text{C}$ transitions at the onset of ETM2. The first transition is marked by an increase in dissolution of $\sim 20\%$, which produces an absolute minimum at least at Site 1267, although it approximates normal background variations, (Figure 6). During this transition, coarse fraction wt % decreased gradually from $\sim 4\%$ to a minimum value of $\sim 0.5\%$ at Sites 1262 and 1267, whereas values remained almost constant at $\sim 2.5\%$ at Sites 1265 and 1263 (Figure 4). An additional 40% dissolution marks the second $\delta^{13}\text{C}$ transition (Figure 6); at this time the coarse fraction wt % of Sites 1262 and 1267 reached minimum values ($< 1\%$), confirming the total dissolution of more than 80% of carbonate at the deepest sites. The coarse fraction wt % of the shallower Sites 1263 and 1265 remained constant also during this transition (Figure 4). Coarse fraction wt % of the shallower sites increased to ~ 4 wt % just before the third $\delta^{13}\text{C}$ transition at the base of the Elmo horizon. Afterward, severe dissolution of more than $> 95\%$ took place at all sites, and the coarse fraction wt % of the shallowest Sites 1263 and 1265 dropped to less than 1% (Figure 4). Recovery of the coarse fraction wt % was almost synchronous between the sites, approximating the recovery phase of the carbonate content at a relative age of ~ 55 ka, with the shallower sites tending to recover slightly faster than the deeper sites.

3.4. Spectral Analysis

[23] All $\delta^{13}\text{C}$ records of the studied sites reveal significant (80%) spectral power in the precession (20–24 ka) and short-eccentricity (~ 115 ka) bands (Figure 7). Site 1267, for which our record is long enough, also shows significant power in the long-eccentricity band. Minor peaks were recorded in some of the spectra around 55, 40 and 29 ka,

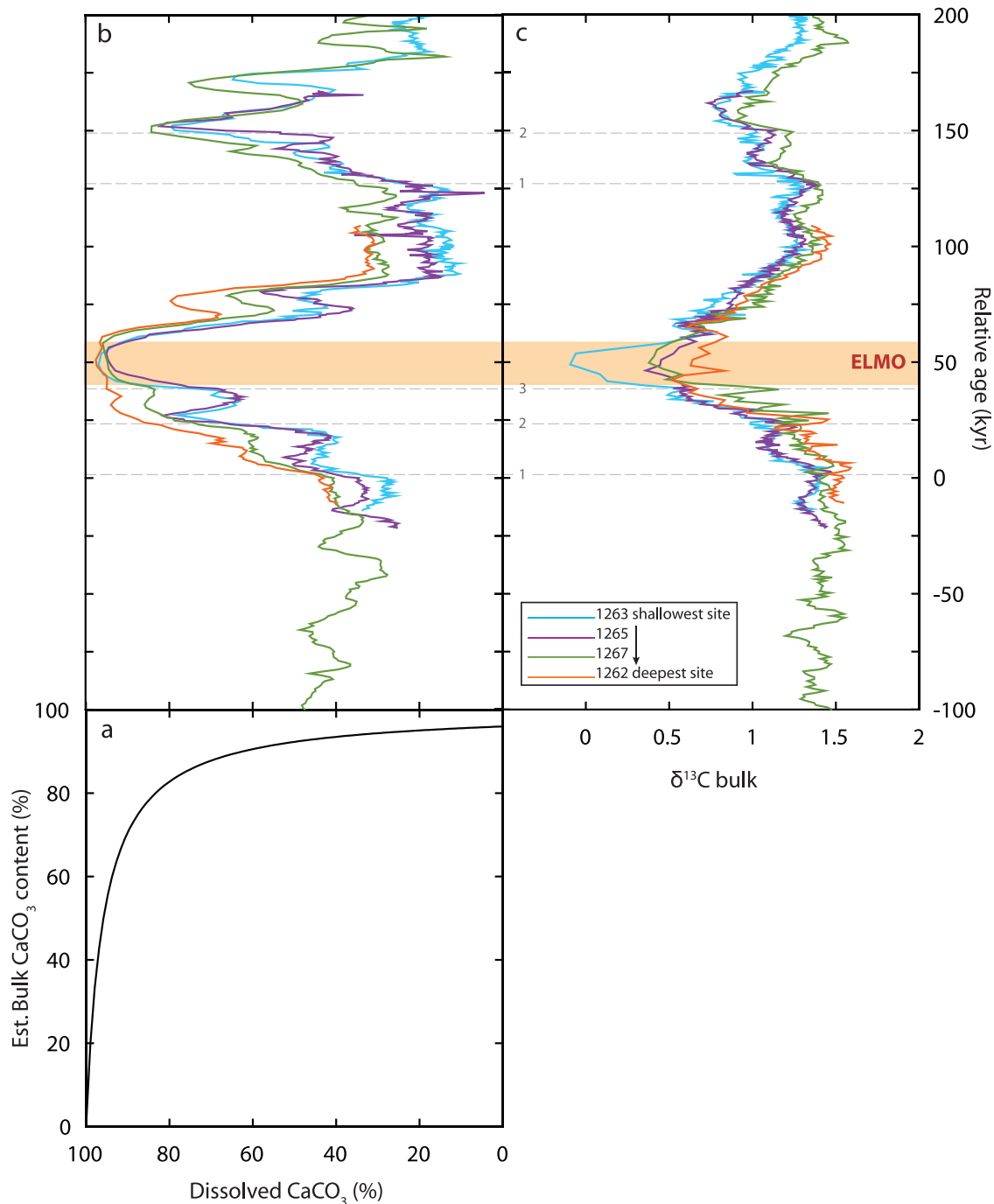


Figure 6. (a) The amount of (estimated) carbonate in the sediment plotted versus the (calculated) dissolved calcite. This graph clearly shows that large amounts of dissolution are required before the calcite content of the sediments drops significantly [Broecker, 1995]. (b) Dissolved calcite content plotted and (c) bulk sediment $\delta^{13}\text{C}$ versus age for Sites 1263, 1265, 1267, and 1262. Gray dotted lines indicate several $\delta^{13}\text{C}$ transitions during the onset of the events.

i.e., the obliquity frequency band. To investigate the imprint of eccentricity and precession on the $\delta^{13}\text{C}$ records we extracted the peaks significant at 99% and 80%, and plotted the resulting signals as overlays to the original time series (Figure 7). The various records reveal 3–5 precession-

related cycles within ETM2, superimposed on the short-term (100–120 ka) eccentricity pacing. The first $\delta^{13}\text{C}$ transition marks one precession cycle, whereas the second and third transitions are merged by one “long” (i.e., extended) precession cycle (Figure 7). In contrast, the

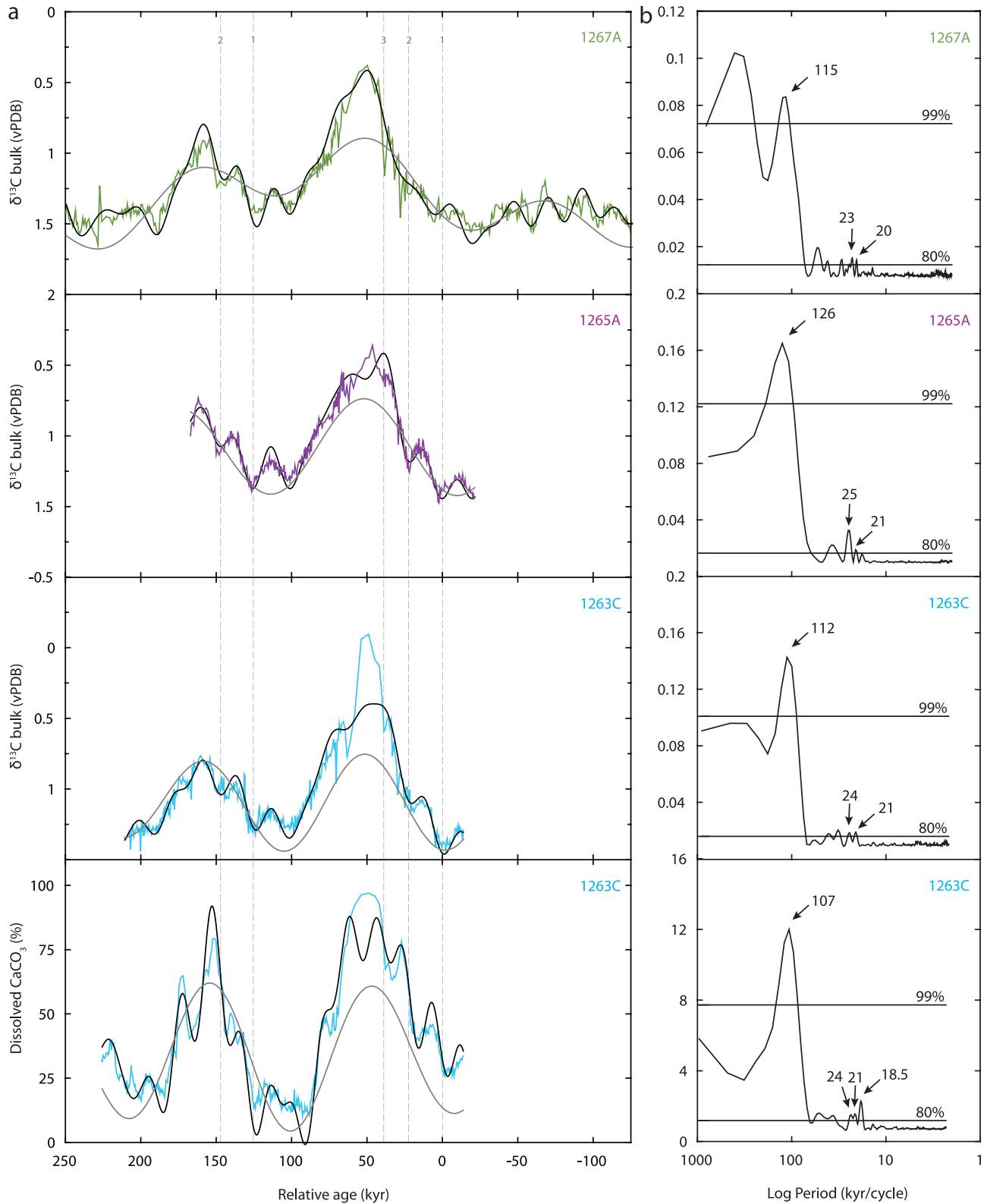


Figure 7. CLEAN spectral results of the bulk $\delta^{13}\text{C}$ records and dissolved carbonate wt %. (a) The extracted precession (black lines) and short-term eccentricity-related (gray lines) components, representing the 99% and 80% significant periods of the CLEAN spectra, respectively. Gray dotted lines indicate several $\delta^{13}\text{C}$ transitions during the onset of the events. (b) The CLEAN frequency spectra (see text for further explanations).

spectral results of the CaCO_3 dissolution record (Figure 7) show two distinct precession-related cycles, which slightly led the three major transitions in the $\delta^{13}\text{C}$ excursion (Figure 7). The recovery phase shows one “long” (i.e., extended) precession cycle in the carbon isotopes, whereas in the CaCO_3 dissolution record the spectral results show two distinct precession-related cycles. Uncertainty in counting the exact number of precession-related cycles encompassing ETM2 arises mainly from the ambiguous recognition of these cycles within the Elmo horizon and to a lesser degree those on the flanks of the CIE (Figure 7): if one would use a slightly different estimate of the terrigenous flux within the Elmo horizon of Site 1263, the spectral results of all sites would be different. For example, a longer (or shorter) duration of the Elmo clay layer will result in more (or less) precession cycles within the Elmo horizon. The H2 event comprises 2–3 precession-related cycles superimposed on the short-term (100–120 ka) eccentricity pacing.

4. Discussion

4.1. Magnitude of the CIE and Temperature Rise During ETM2 and H2

[24] The major constituents of the pelagic sediments at Walvis Ridge are calcareous nannofossils. The bulk $\delta^{13}\text{C}$ records therefore reflect primarily the isotopic composition of the total dissolved inorganic carbon in the lower photic zone where these organisms dominantly calcify [Thomas *et al.*, 2002; Stoll, 2005]. All studied sites are in close proximity, thus underlying the same surface water masses, and bulk isotopic values of exported calcite should be the same at all sites. However, the bulk carbon isotope records show a depth-dependent increase in their mean values over the whole studied interval. Moreover, there was an additional excursion within the Elmo horizon at Site 1263 (Figure 4).

[25] It is generally assumed that the carbon isotope signal is not much affected by diagenesis (as shown for planktonic foraminifera) [Sexton *et al.*, 2006] or burial depth [Schrag *et al.*, 1995]. Partial dissolution, on the other hand, may have caused an increase in relative abundance of solution-resistant taxa of nannofossils in PETM sediments, such as *Discoaster*, *Sphenolithus* and *Ericsonia* [Gibbs *et al.*, 2004; Tremolada and Bralower, 2004; Stoll *et al.*, 2007; Raffi and De Bernardi, 2008]. Modern species of nannoplankton differ in isotopic signature, so that changes in assemblage composition, but also selective dissolution, may lead to a change in average isotopic value of bulk carbonate [Ziveri *et al.*, 2003]. At Site 690, for instance, partial dissolution during the PETM may have biased the oxygen and carbon isotopes of the bulk sediment by up to 0.5‰ [Stoll, 2005]. Even outside ETM2 and H2, more carbonate dissolved at the deeper sites than at the shallower sites (Figure 6). If this dissolution was selective, it might explain the depth dependence of the average bulk carbon isotopic composition across the studied interval. It may also explain the gradual decline in $\delta^{18}\text{O}$ values by 0.2‰ from the shallower sites to the deeper sites during ETM2 (Figure 5), when carbonate dissolution was at a maximum. This $\delta^{18}\text{O}$ gradient

is absent during H2 (Figure 5), which is marked by much less severe carbonate dissolution.

[26] It remains uncertain why the additional $\delta^{13}\text{C}$ transition and associated $\delta^{18}\text{O}$ excursion, recorded at Site 1263, is absent from the deeper sites. This may have been caused by truncation or by dissolution (i.e., an unconformity), as found for the PETM [Zachos *et al.*, 2005; McCarren *et al.*, 2008], but the additional excursion at Site 1263 could also have been caused by an overprint of an abiotic (authigenic) carbonate source [Lourens *et al.*, 2005]. Physical evidence for an unconformity has not been found within the Elmo horizon of the deep sites, but this could have been masked by bioturbation.

[27] Thus, the magnitude of the CIE during ETM2 differs between the bulk records of the deeper Sites 1262, 1265, 1267 ($\sim 1.0\%$) and the shallowest Site 1263 ($\sim 1.5\%$), whereas no discrepancy was found between the studied sites for the CIE of H2 ($\sim 0.6\%$). Notwithstanding these uncertainties, the CIE during ETM2 and H2 at Walvis Ridge are amplified with respect to the 0.6–1.0‰ and 0.2–0.4‰ found at other locations [e.g., Cramer *et al.*, 2003; Nicolo *et al.*, 2007]. The CIE of Site 1263 as recorded in the surface dweller *Acarinina* is 2.5‰, while the benthic foraminifera *Anomalinoidea* records a CIE of 1‰ in the deep sea, although it is unclear whether these benthic specimens were bioturbated or in situ [Lourens *et al.*, 2005]. These large differences as yet prohibit an accurate estimate of the global mass and source of carbon released during these events. A CIE range of 0.6–2.5‰ during ETM2 might be explained for instance by a release of ~ 400 –1600 Gt of carbon with a $\delta^{13}\text{C}$ -60% (methane) or a release of ~ 1000 –4500 Gt of carbon with a $\delta^{13}\text{C}$ -22% (organic carbon), assuming a exchangeable carbon reservoir of 38000 Gt [Dickens, 2001; Ridgwell, 2007].

[28] It was previously shown that the CIE of ETM2 is accompanied by a decrease in the $\delta^{18}\text{O}$ of the surface dwelling planktonic foraminifer *Acarinina soldadoensis* of 1‰, suggesting a sea surface temperature (SST) rise of at least 3–4°C [Lourens *et al.*, 2005], about half the middle- to high-latitude sea surface temperature changes estimated for the PETM [Kennett and Stott, 1991; Thomas *et al.*, 2002; Zachos *et al.*, 2003]. The bulk $\delta^{18}\text{O}$ drop during H2 of 0.5‰ is about half to one third the bulk $\delta^{18}\text{O}$ excursion of -0.7 to -1.5% during ETM2, which may imply a maximum SST rise of 1–2°C.

4.2. CaCO_3 Dissolution

[29] A massive and rapid injection of CO_2 into the ocean and atmosphere will decrease seawater pH and $[\text{CO}_3^{2-}]$, shoaling of the lysocline and calcite compensation depth (CCD), and dissolution of sedimentary carbonate in the deep ocean [Dickens *et al.*, 1997]. The depth transect of sites on Walvis Ridge revealed a CCD shoaling of more than 2 km within a few thousand years during the PETM [Zachos *et al.*, 2005]. Recovery was gradual, with the fastest return to carbonate preservation at the shallowest Site 1263 after ~ 10 to 15 ka of the CIE onset, and the slowest recovery of ~ 60 ka at the deepest Site 1262. By ~ 110 ka, carbonate content had fully recovered at all sites, including a period of “overcompensation” during which the

lysocline was located deeper than prior to the event, resulting from $[\text{CO}_3^{2-}]$ oversaturation [Dickens *et al.*, 1997; Zachos *et al.*, 2005]. Ridgwell [2007] used an intermediate Earth System complexity model (GENIE-1) to simulate the observed changes in carbonate content at Walvis Ridge, and showed that a reduction in bioturbation and a rapid release (<1 ka) of carbon are important factors determining the (asymmetric) shape of the carbonate content record. However, this model, using a single injection at the onset of the event, underestimates the total duration of the PETM [Ridgwell, 2007], and cannot properly simulate the relative duration of the dissolution horizon at the different sites.

[30] The quasi-symmetric carbonate content patterns of ETM2 and H2 (Figure 4) differ significantly from the asymmetric saw-tooth pattern of the records at the PETM, but the dissolution of CaCO_3 occurred synchronously between the sites (Figure 6), indicating that changes in the carbonate content are the result of lysocline migration through the water column. The quasi-symmetric shape of records during ETM2 and H2 may be due to the smaller amount of carbon released during these events than during the PETM. Taking the experiments with an injection of 4500 Pg of C [Ridgwell, 2007] as an upper limit for the carbon release during ETM2, one might expect a maximum duration of the CaCO_3 dissolution and recovery interval of ~30 ka [see Ridgwell, 2007, Figure 5]. In contrast, however, our age model shows a total duration for ETM2 of about 100 ka (Figure 7). One possible explanation for this could be that the carbon input did not comprise one single injection but consisted of multiple pulses. This hypothesis is supported by the concurrence of several precession-paced (~20 ka apart) transitions in our $\delta^{13}\text{C}$ and CaCO_3 dissolution records throughout the first 40 ka of ETM2 and the onset of H2. Such a mechanism would extend the total duration of dissolution and recovery compared to the simulated scenarios, which include only a single (rapid) release. Also, there is physical evidence for bioturbation (as revealed in the core photos and as observed during sampling), which might have smoothed the signal, resulting in an overestimate of the time spanning the onset and recovery and an underestimate of the maximum amount of carbonate dissolved, particularly within the Elmo horizon.

[31] Apparently, the $\delta^{13}\text{C}$ and CaCO_3 dissolution pattern during ETM2 and H2 reflects the cumulative imprint of a succession of precession-paced carbon inputs into the ocean and atmosphere. This brings up the question how to discriminate between an anomalous event (i.e., methane release) and the regular precession-paced background variations in the early Eocene carbon cycle. In this respect one could argue that the first $\delta^{13}\text{C}$ transition and associated carbonate dissolution of up to ~60% at the onset of ETM2 and H2 reflects an average background, precession-paced, perturbation in the carbon cycle, while during the successive transitions additional carbon input from also other sources, such as methane hydrates, may have driven the climate to much warmer conditions through enhanced greenhouse gas concentrations and caused severe carbonate dissolution of more than ~80% in the deep sea.

4.3. CIE Recovery Phase and Weathering Feedbacks

[32] The leading hypothesis to explain the recovery of the lysocline during the PETM is silicate weathering [Dickens *et al.*, 1997; Ravizza *et al.*, 2001; Kelly *et al.*, 2005; Zachos *et al.*, 2005]. This mechanism, however, is less effective on time scales shorter than 100 ka [Ridgwell and Zeebe, 2005]. This suggests that silicate weathering was not the primary mechanism to explain the ~30 ka recovery period of ETM2 after deposition of the Elmo horizon. For the modern and future fossil fuel CO_2 injection, terrestrial CaCO_3 neutralization, i.e., weathering of carbonates in soils and at exposed rock surfaces, is expected to renew the ocean $[\text{CO}_3^{2-}]$ and to bring down the lysocline on short (<20 ka) time scales [Archer *et al.*, 1998; Ridgwell and Edwards, 2007]. Silicate weathering will remove the remaining small amount (~8%) of the CO_2 added to the atmosphere, as well as the 92% of the CO_2 stored in the oceans as HCO_3^- [Archer *et al.*, 1998; Ridgwell and Edwards, 2007]. The rapid recovery of the carbonate system after deposition of the Elmo horizon suggests that terrestrial CaCO_3 neutralization was the driving mechanism.

[33] One might expect that the evolution of the average carbon isotopic signature of the global exogenic carbon reservoir after a massive input of ^{13}C -depleted carbon would be dependent upon and, hence, similar in character to the burial of carbonate in the deep ocean. To further explore the relationship between CaCO_3 dissolution and bulk $\delta^{13}\text{C}$ changes we plotted scatter diagrams between both variables across ETM2 (0 to 100 ka) for each site (Figure 8). These plots reveal that the recovery of CaCO_3 to preevent levels was much faster than the recovery of $\delta^{13}\text{C}$ values, which is model predicted [Dickens *et al.*, 1997] and shown for the PETM [Zachos *et al.*, 2005]. Additionally, similar to the PETM, the CaCO_3 content was even higher during the final phase of the recovery (>85 ka, Figure 8) than prior to ETM2. Apparently, higher CO_2 concentrations and temperatures increased chemical weathering of carbonate rocks (enhancing alkalinity) to supply excess CO_3^{2-} ions to the ocean. This caused rapid recovery of the lysocline and dilution of the injected ^{13}C -depleted carbon. As a result of this model-expected $[\text{CO}_3^{2-}]$ oversaturation [Dickens *et al.*, 1997], the lysocline descended to a deeper position than prior to the event. A gradual sequestration of the excess ^{13}C -depleted carbon through burial, as generally inferred to explain the long (>100 ka) exponential shape of the recovery phase of the PETM [e.g., Dickens *et al.*, 1997; Zachos *et al.*, 2005], appears to have operated for only ~50 ka during the recovery phases of ETM2 and H2.

[34] Evidently, the general trend between dissolution and bulk $\delta^{13}\text{C}$ at all sites is superimposed by the precession-paced perturbations throughout ETM2 (Figure 8). In contrast to the onset of ETM2 and H2, during the recovery these superimposed variations are in particularly related to CaCO_3 preservation and lysocline depth, rather than to changes in $\delta^{13}\text{C}$ (Figures 6 and 8). This suggests that ocean alkalinity during the early Eocene was, in addition to the precession-induced perturbations in the carbon cycle, highly responsive to weathering intensity variations. This is in agreement with the pronounced precession-paced color

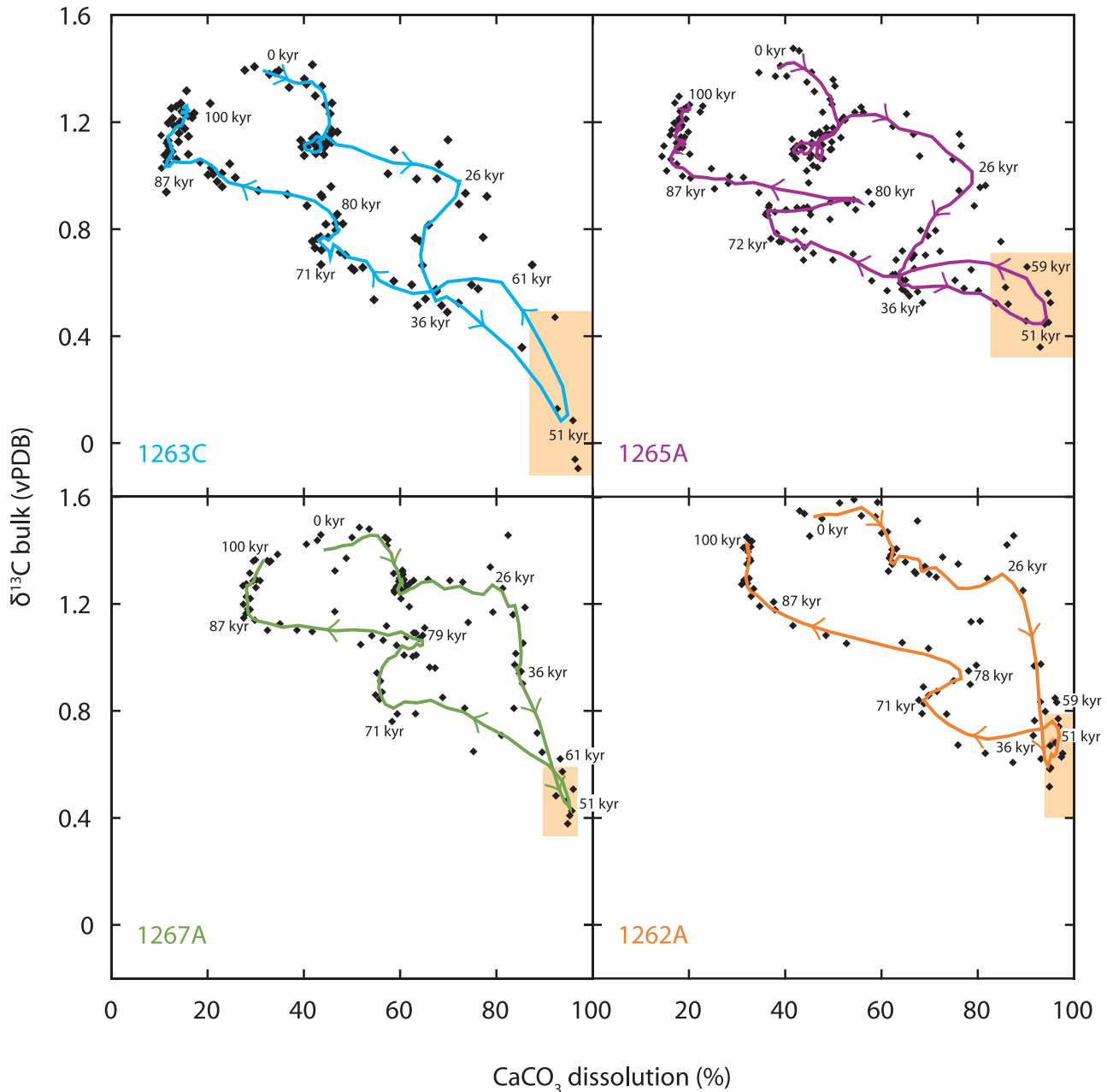


Figure 8. Scatterplots between CaCO_3 dissolution % and bulk $\delta^{13}\text{C}$ for ETM2 for Sites 1263, 1265, 1267, and 1262. Lines represent a five point moving average. The marked square indicates the Elmo clay layer.

cycles in the interval between the PETM and ETM2 [Lourens *et al.*, 2005; Westerhold *et al.*, 2007].

[35] **Acknowledgments.** This research used samples and data provided by the Integrated Ocean Drilling Program (IODP). Funding for this research was provided by the Darwin Centre for Biogeology to L. Stap, by the Netherlands Organisation for Scientific Research (NWO) through VENI

grant 863.07.001 to A. Sluijs, and by NSF grant EAR-010727 to E. Thomas. We also thank NWO for their continued support of the IODP. We thank D. Liebrand, A. van Dijk, G. Ittman, J. Heijdt, and T. Evers for technical support and Dick Kroon, Jim Zachos, and Martin Ziegler for discussions. We are grateful to Deborah Thomas, Andy Ridgwell, and Gerald Dickens for thorough and constructive reviews of an earlier version of this manuscript.

References

- Archer, D., H. Kheshgi, and E. Maier-Reimer (1998), Dynamics of fossil fuel CO_2 neutralization by marine CaCO_3 , *Global Biogeochem. Cycles*, 12, 259–276, doi:10.1029/98GB00744.
- Broecker, W. S. (1995), *The Glacial World According to Wally*, Eldigio, Palisades, N. Y.
- Clemens, S. C., and W. L. Prell (1991), One million year record of summer monsoon winds and continental aridity from the Owen Ridge (Site 722), northwest Arabian sea, *Proc. Ocean Drill. Program Sci. Results*, 117, 365–388.
- Cramer, B. S., J. D. Wright, D. V. Kent, and M.-P. Aubry (2003), Orbital climate forcing of $\delta^{13}\text{C}$ excursions in the late Paleocene–early Eocene

- (chrons C24n–C25n), *Paleoceanography*, 18(4), 1097, doi:10.1029/2003PA000909.
- Dickens, G. (2001), Carbon addition and removal during the Late Palaeocene Thermal Maximum: Basic theory with a preliminary treatment of the isotope record at ODP Site 1051, Blake Nose, in *Western North Atlantic Paleogene and Cretaceous Paleoclimatology*, edited by D. Kroon et al., *Geol. Soc. Spec. Publ.*, 183, 293–305.
- Dickens, G. R., J. R. O’Neil, D. K. Rea, and R. M. Owen (1995), Dissociation of oceanic methane hydrate as a cause of the carbon isotope excursion at the end of the Paleocene, *Paleoceanography*, 10, 965–971, doi:10.1029/95PA02087.
- Dickens, G. R., M. M. Castillo, and J. C. Walker (1997), A blast of gas in the latest Paleocene: Simulating first-order effects of massive dissociation of oceanic methane hydrate, *Geology*, 25, 259–262, doi:10.1130/0091-7613(1997)025<0259:ABOGIT>2.3.CO;2.
- Gibbs, S. J., N. J. Shackleton, and J. R. Young (2004), Identification of dissolution patterns in nannofossil assemblages: A high-resolution comparison of synchronous records from Ceara Rise, ODP Leg 154, *Paleoceanography*, 19, PA1029, doi:10.1029/2003PA000958.
- Hancock, H. J. L., and G. R. Dickens (2006), Carbonate dissolution episodes in Paleocene and Eocene sediment, Shatsky Rise, west-central Pacific [online], *Proc. Ocean Drill. Program Sci. Results*, 198, 24 pp. (Available at http://www-odp.tamu.edu/publications/198_SR/VOLUME/CHAPTERS/116.PDF)
- Heslop, D., and M. J. Dekkers (2002), Spectral analysis of unevenly spaced climatic time series using CLEAN: Signal recovery and derivation of significance levels using a Monte Carlo simulation, *Phys. Earth Planet. Inter.*, 130, 103–116, doi:10.1016/S0031-9201(01)00310-7.
- Higgins, J. A., and D. P. Schrag (2006), Beyond methane: Towards a theory for the Paleocene–Eocene Thermal Maximum, *Earth Planet. Sci. Lett.*, 245, 523–537, doi:10.1016/j.epsl.2006.03.009.
- Kelly, D. C., J. C. Zachos, T. J. Bralower, and S. A. Schellenberg (2005), Enhanced terrestrial weathering/runoff and surface ocean carbonate production during the recovery stages of the Paleocene-Eocene thermal maximum, *Paleoceanography*, 20, PA4023, doi:10.1029/2005PA001163.
- Kennett, J. P., and L. D. Stott (1991), Abrupt deep-sea warming, palaeoceanographic changes and benthic extinctions at the end of the Paleocene, *Nature*, 353, 225–229, doi:10.1038/353225a0.
- Kurtz, A. C., L. R. Kump, M. A. Arthur, J. C. Zachos, and A. Paytan (2003), Early Cenozoic decoupling of the global carbon and sulfur cycles, *Paleoceanography*, 18(4), 1090, doi:10.1029/2003PA000908.
- Lourens, L. J., A. Sluijs, D. Kroon, J. C. Zachos, E. Thomas, U. Röhl, J. Bowles, and I. Raffi (2005), Astronomical pacing of late Palaeocene to early eocene global warming events, *Nature*, 435, 1083–1087, doi:10.1038/nature03814.
- McCarren, H., E. Thomas, T. Hasegawa, U. Röhl, and J. C. Zachos (2008), Depth dependency of the Paleocene-Eocene carbon isotope excursion: Paired benthic and terrestrial biomarker records (Ocean Drilling Program Leg 208, Walvis Ridge), *Geochem. Geophys. Geosyst.*, 9, Q10008, doi:10.1029/2008GC002116.
- Moore, E. A., and A. C. Kurtz (2008), Black carbon in Paleocene-Eocene boundary sediments: A test of biomass combustion as the PETM trigger, *Palaeogeogr. Palaeoclimatol. Palaeoecol.*, 267, 147–152, doi:10.1016/j.palaeo.2008.06.010.
- Nicolo, M., and G. R. Dickens (2006), Data report: Terrigenous grain-size distributions at Sites 1263 and 1267: Testing the applicability of Leg 208 sediments for eolian analysis [online], *Proc. Ocean Drill. Program Sci. Results*, 208, 13 pp. (Available at http://www-odp.tamu.edu/publications/208_SR/VOLUME/CHAPTERS/205.PDF)
- Nicolo, M. J., G. R. Dickens, C. J. Hollis, and J. C. Zachos (2007), Multiple early Eocene hyperthermals: Their sedimentary expression on the New Zealand continental margin and in the deep sea, *Geology*, 35, 699–702, doi:10.1130/G23648A.1.
- Pagani, M., K. Caldeira, D. Archer, and J. C. Zachos (2006), An ancient carbon mystery, *Science*, 314, 1556–1557, doi:10.1126/science.1136110.
- Panchuk, K., A. Ridgwell, and L. R. Kump (2008), Sedimentary response to Paleocene-Eocene Thermal Maximum carbon release: A model-data comparison, *Geology*, 36, 315–318, doi:10.1130/G24474A.1.
- Raffi, I., and B. De Bernardi (2008), Response of calcareous nannofossils to the Paleocene–Eocene Thermal Maximum: Observations on composition, preservation and calcification in sediments from ODP Site 1263 (Walvis Ridge–SW Atlantic), *Mar. Micropaleontol.*, 69, 119–138, doi:10.1016/j.marmicro.2008.07.002.
- Ravizza, G., R. N. Norris, J. Blusztajn, and M. P. Aubry (2001), An osmium isotope excursion associated with the late Paleocene thermal maximum: Evidence of intensified chemical weathering, *Paleoceanography*, 16, 155–163, doi:10.1029/2000PA000541.
- Ridgwell, A. (2007), Interpreting transient carbonate compensation depth changes by marine sediment core modeling, *Paleoceanography*, 22, PA4102, doi:10.1029/2006PA001372.
- Ridgwell, A., and U. Edwards (2007), Geological carbon sinks, in *Greenhouse Gas Sinks*, edited by D. S. Reay et al., pp. 74–97, CABI, Wallingford, U. K.
- Ridgwell, A., and R. E. Zeebe (2005), The role of the global carbonate cycle in the regulation and evolution of the Earth system, *Earth Planet. Sci. Lett.*, 234, 299–315, doi:10.1016/j.epsl.2005.03.006.
- Roberts, D. H., J. Lehar, and J. W. Dreher (1987), Time series analysis with CLEAN. 1. Derivation of a spectrum, *Astron. J.*, 93, 968–989, doi:10.1086/114383.
- Schlanger, S. O., and R. G. Douglas (1974), The pelagic ooze-chalk-limestone transition and its implication for marine stratigraphy, in *Pelagic Sediments: On Land and Under the Sea*, edited by K. J. Hsü and H. C. Jenkyns, *Spec. Publ. Int. Assoc. Sedimentol.*, 1, 117–148.
- Schouten, S., M. Woltering, W. I. C. Rijpstra, A. Sluijs, H. Brinkhuis, and J. S. S. Damste (2007), The Paleocene-Eocene carbon isotope excursion in higher plant organic matter: Differential fractionation of angiosperms and conifers in the Arctic, *Earth Planet. Sci. Lett.*, 258, 581–592, doi:10.1016/j.epsl.2007.04.024.
- Schrag, D. P., D. J. Depaolo, and F. M. Richter (1995), Reconstructing past sea surface temperatures: Correcting for diagenesis of bulk marine carbonate, *Geochim. Cosmochim. Acta*, 59, 2265–2278, doi:10.1016/0016-7037(95)00105-9.
- Sexton, P. F., P. A. Wilson, and P. N. Pearson (2006), Microstructural and geochemical perspectives on planktic foraminiferal preservation: “Glassy” versus “Frosty”, *Geochem. Geophys. Geosyst.*, 7, Q12P19, doi:10.1029/2006GC001291.
- Sluijs, A., G. J. Bowen, H. Brinkhuis, L. J. Lourens, and E. Thomas (2007a), The Palaeocene-Eocene Thermal Maximum super greenhouse: Biotic and geochemical signatures, age models and mechanisms of global change, in *Deep-Time Perspectives on Climate Change: Marrying the Signal From Computer Models and Biological Proxies*, edited by M. Williams et al., pp. 323–349, Geol. Soc. of London, London.
- Sluijs, A., H. Brinkhuis, S. Schouten, S. M. Bohaty, C. M. John, J. C. Zachos, G. J. Reichart, J. S. S. Damste, E. M. Crouch, and G. R. Dickens (2007b), Environmental precursors to rapid light carbon injection at the Palaeocene/Eocene boundary, *Nature*, 450, 1218–1221, doi:10.1038/nature06400.
- Sluijs, A., U. Röhl, S. Schouten, H.-J. Brumsack, F. Sangiorgi, J. S. S. Damsté, and H. Brinkhuis (2008), Arctic late Paleocene–early Eocene paleoenvironments with special emphasis on the Paleocene-Eocene thermal maximum (Lomonosov Ridge, Integrated Ocean Drilling Program Expedition 302), *Paleoceanography*, 23, PA1S11, doi:10.1029/2007PA001495.
- Stoll, H. M. (2005), Limited range of interspecific vital effects in coccolith stable isotopic records during the Paleocene-Eocene thermal maximum, *Paleoceanography*, 20, PA1007, doi:10.1029/2004PA001046.
- Stoll, H. M., N. Shimizu, D. Archer, and P. Ziveri (2007), Coccolithophore productivity response to greenhouse event of the Paleocene-Eocene Thermal Maximum, *Earth Planet. Sci. Lett.*, 258, 192–206, doi:10.1016/j.epsl.2007.03.037.
- Svensen, H., S. Planke, A. Malthes-Sørensen, B. Jamtveit, R. Myklebust, T. R. Eidem, and S. S. Rey (2004), Release of methane from a volcanic basin as a mechanism for initial Eocene global warming, *Nature*, 429, 542–545, doi:10.1038/nature02566.
- Thomas, D. J., J. C. Zachos, T. J. Bralower, E. Thomas, and S. Bohaty (2002), Warming the fuel for the fire: Evidence for the thermal dissociation of methane hydrate during the Paleocene-Eocene thermal maximum, *Geology*, 30, 1067–1070, doi:10.1130/0091-7613(2002)030<1067:WTFFTF>2.0.CO;2.
- Thomas, E., and N. J. Shackleton (1996), The Paleocene-Eocene benthic foraminiferal extinction and stable isotope anomalies, in *Correlation of the Early Paleogene in Northwest Europe*, edited by R. W. O. B. Knox et al., *Geol. Soc. Spec. Publ.*, 101, 401–411.
- Thomas, E., and J. C. Zachos (2000), Was the late Paleocene thermal maximum a unique event?, *GFF*, 122, 169–170.
- Tremolada, F., and T. J. Bralower (2004), Nannofossil assemblage fluctuations during the Paleocene-Eocene Thermal Maximum at Sites 213 (Indian Ocean) and 401 (North Atlantic Ocean): Palaeoceanographic implications, *Mar. Micropaleontol.*, 52, 107–116, doi:10.1016/j.marmicro.2004.04.002.
- Verosub, K. L., and A. P. Roberts (1995), Environmental magnetism: Past, present and future, *J. Geophys. Res.*, 100, 2175–2192, doi:10.1029/94JB02713.
- Westerhold, T., U. Röhl, J. Laskar, I. Raffi, J. Bowles, L. J. Lourens, and J. C. Zachos (2007), On the duration of magnetochrons

- C24r and C25n and the timing of early Eocene global warming events: Implications from the Ocean Drilling Program Leg 208 Walvis Ridge depth transect, *Paleoceanography*, 22, PA2201, doi:10.1029/2006PA001322.
- Zachos, J. C., K. C. Lohmann, J. C. G. Walker, and S. W. Wise (1993), Abrupt climate change and transient climates during the Paleogene—A marine perspective, *J. Geol.*, 101, 191–213.
- Zachos, J. C., M. W. Wara, S. Bohaty, M. L. Delaney, M. R. Petrizzo, A. Brill, T. J. Bralower, and I. Premoli-Silva (2003), A transient rise in tropical sea surface temperature during the Paleocene-Eocene Thermal Maximum, *Science*, 302, 1551–1554, doi:10.1126/science.1090110.
- Zachos, J. C., et al. (2004), *Proceedings of the Ocean Drilling Program, Initial Reports*, vol. 208, Ocean Drill. Program, College Station, Tex.
- Zachos, J. C., et al. (2005), Rapid acidification of the ocean during the Paleocene-Eocene thermal maximum, *Science*, 308, 1611–1614, doi:10.1126/science.1109004.
- Ziveri, P., H. Stoll, I. Probert, C. Klass, M. Geisen, G. Ganssen, and J. Young (2003), Stable isotope vital effects in coccolith calcite, *Earth Planet. Sci. Lett.*, 210, 137–149, doi:10.1016/S0012-821X(03)00101-8.
-
- L. Lourens and L. Stap, Faculty of Geosciences, Utrecht University, Budapestlaan 4, NL-3584 CD Utrecht, Netherlands. (stap@geo.uu.nl)
- A. Sluijs, Palaeoecology, Laboratory of Palaeobotany and Palynology, Institute of Environmental Biology, Utrecht University, Budapestlaan 4, NL-3584 CD Utrecht, Netherlands.
- E. Thomas, Centre for the Study of Global Change, Department of Geology and Geophysics, Yale University, New Haven, CT 06520-8109, USA.